Casting Defects in Low-Pressure Die-Cast Aluminum Alloy Wheels

B. Zhang, S.L. Cockcroft, D.M. Maijer, J.D. Zhu, and A.B. Phillion

Defects in automotive aluminum alloy casting continue to challenge metallurgists and production engineers as greater emphasis is placed on product quality and production cost. A range of casting-related defects found in low-pressure die-cast aluminum wheels were examined metallographically in samples taken from several industrial wheel-casting facilities. The defects examined include macro- and micro- porosity, entrained oxide films, and exogenous oxide inclusions. Particular emphasis is placed on the impact of these defects with respect to the three main casting-related criteria by which automotive wheel quality are judged: wheel cosmetics, air-tightness, and wheel mechanical performance.

INTRODUCTION

The auto industry is moving toward increased usage of lightweight aluminum alloy castings for many components previously made from steel and cast iron. Examples include cylinder heads, engine blocks, suspension components, brake components, and wheels. In the case of wheels, cast aluminum alloys offer improved aesthetic appearance and design flexibility over the traditional stamped and welded steel product. As a result, most new North American cars are equipped with cast aluminum wheels.[1] Within the wheel industry, style trends include greater emphasis on machined face wheels, high-luster paints, open-faced wheels with smaller spoke areas, and larger-diameter wheels.

Among automotive castings, the wheel is somewhat unique as it must meet or exceed a combination of requirements. These include impact and fatigue performance, as wheels are critical safety components and their failure can result in injury or death of vehicle occupants;[2] air tightness, as the rim is required to serve as one component of a pressure vessel in conjunction with the tire; high-quality surface finish, as wheels are one of the prominent cosmetic features on cars; and geometric and rotational balance tolerances, which are becoming more stringent. In the context of these requirements, the term defect constitutes any feature arising from the manufacturing process that necessitates repair or rejection of the wheel. Many casting-related defects continue to challenge metallurgists and manufacturing engineers, particularly since market pressures demand improvements in product quality and expansion of the design envelope while at the same time reducing costs. The formation and prediction of these defects, along with methods to remove them, are the focus of this paper.

WHEEL CASTING PROCESSES

Owing to its ability to produce high-quality wheels in a cost-effective manner, the dominant process for casting aluminum alloy wheels is the low-pressure die-casting process (LPDC). A typical LPDC casting machine comprises a die assembly containing two die cavities located above an electrically heated holding furnace. The dies are typically made from a combination of tool steel and cast iron. Each die cavity is geometrically complex, with four sections as shown in Figure 1: a bottom die, two side dies, and a top die. The casting process is cyclic and begins with the pressurization of the furnace, which contains a reservoir of molten aluminum. The excess pressure in the holding furnace forces liquid aluminum up into the die cavity, where it is cooled and solidified by the transfer of heat from the aluminum to the die and then out to the environment. After solidification is complete, the side dies open and the top die is raised vertically. The wheel remains fixed to the top die (owing to thermal contraction) for a short time and is then ejected onto a transfer tray rolled under the top die. The die is then closed and the cycle restarted. Typical cycle times are 5 min. to 6 min. Following the casting operation, the wheels are typically rough machined, heat treated, finished, machined, and painted.

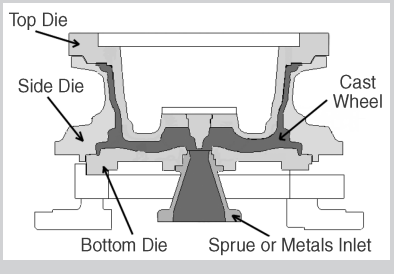

Figure 1. A die-tooling assembly for typical LPDC process.

During solidification, control of cooling rates is important for product quality. In the bottom die, cooling is augmented by forcing air through internal channels at various times during the casting cycle. In the top die, cooling is controlled by air jets aimed at various sections of the exterior face. On the side dies, cooling may be retarded by the addition of insulation to the cold face at certain locations or augmented by air cooling, depending on the casting conditions.

See the sidebar for experimental procedures.

RESULTS AND DISCUSSIONS

In any manufacturing process, defects are dependent on the tolerances that exist within that process. In essence, a feature of the manufacturing process becomes a defect when its presence results in the product failing to meet the prevailing

a

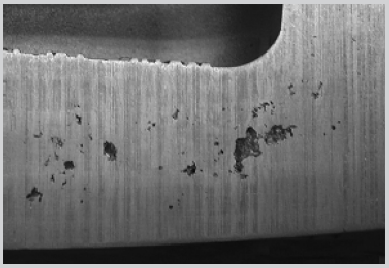

b 20 mm

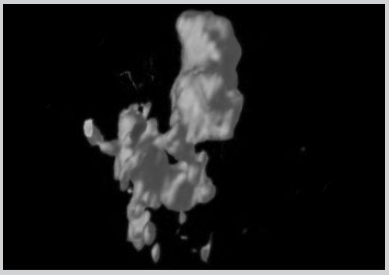

c

Figure 2. An example of macroporosity clusters in a wheel: (a) a macroscopic x-ray image of hub area showing macroporosity cluster; (b) a sectioned spoke showing macroporosity cluster; (c) a two-dimensional x-ray projection of macroporosity cluster.

quality control standards. In the case of wheels, the casting is typically rejected for one of three reasons: failure to meet the cosmetic appearance criteria (cosmetic defects); failure to meet the mechanical criteria (generally fatigue and impact properties); and failure to meet the pressurization criteria (rim-leak defects, as the rim flange fails to hold air when fitted with a tire). Of these three quality-control tests, control for cosmetic appearance is generally the most difficult. However, wheels failing this criterion can often be repaired instead of being scrapped and remelted. In contrast, rim-leak defects cannot be repaired; wheels failing this criterion must be scrapped and remelted at considerable expense since this defect can only be tested following final machining. An evaluation of the mechanical criteria usually occurs in the preproduction stage, during development of the wheel and die assembly. Failure to meet the mechanical criteria can lead to a redesign of the wheel and die tooling, an extremely costly process.

A number of features of the casting process can result in the wheel failing to meet the quality-control standard, including macroporosity, microporosity, oxide films, and oxide inclusions. The remainder of this article focuses on each of these defects in terms of understanding their formation during the casting process, effect on quality, and reducing their occurrence.

Macroporosity

Macro- or shrinkage porosity forms in locations where there is insufficient feeding of liquid metal to offset the volumetric shrinkage associated with the solid-to-liquid transformation. This shrinkage is approximately 4% by volume in A356, a common alloy used for wheel castings. Figure 2 shows a good example of macroporosity clusters within a hub and spoke section. This porosity formed because directional solidification was lost, resulting in liquid being encapsulated by solid. This feature impacts greatly on load bearing, fatigue, and impact performance. For each wheel model and manufacturing process, specific tolerances for macroporosity in each section of the wheel must be set. Other common instances in which macroporosity constitutes a defect include porosity intersecting the surface, as this can lead to cosmetic defects, and interconnected porosity in the rim flange, as this can provide a pathway for air and create a rim-leak defect. The most common location for macroporosity is found in the region where the spoke and rim intersect. Most aluminum wheel designs tolerate some macroporosity in this region.

The most significant recent advancement in controlling macroporosity is the use of computer-based heat flow simulations of both the solidifying wheel and the LPDC die. This allows dies to be designed properly, ensuring directional solidification and thus avoiding the primary cause of macroporosity: substantial liquid metal entrapment. The major challenges remaining for these simulations are twofold. First, better characterization of the boundary conditions is needed to quantify the heat transport in the various components of the die (including the die-wheel interface, the die-die interfaces, and the die-ambient environment interfaces). Unfortunately, relatively little work of this type has been published, since much of it contains proprietary process details. Second, a better ability to quantitatively predict macroporosity distributions from temperature is required.

One area requiring much development, of a more fundamental nature, is the influence of hydrogen content and alloy modification on macroporosity. For example, it is well known within the foundry industry that excessively low hydrogen contents can lead to increased occurrences of macroporosity. Likewise, it is known that alloy modification can influence mass transport within the interdendritic liquid, which will also alter the tendency for macroporosity to form.[3] However, little quantitative work has been reported on these topics.

EXPERIMENTAL PROCEDURES

The method of analysis involved a detailed metallographic investigation of example surface and internal defects taken from strontium-modified A356 aluminum alloy wheels manufactured at a number of casting operations in North America. In the case of surface defects, the samples were first analyzed using an optical microscope to characterize the macroscopic appearance of the defect. These samples were then cut perpendicular to the surface and in proximity to the defect. Additionally, sections of wheels from critical locations were extracted to assess typical internal defects. All of the samples were then mounted in epoxy for grinding and polishing. The grinding was undertaken using sequentially finer and finer grits of SiC paper and then polished using colloidal silica. In the case of surface defect samples, a very careful step-by step approach to grinding and polishing was conducted to ensure that both the surface defect and the underlying structure were preserved and exposed to view.

The samples were photographed using a Nikon SMZ-1000 optical microscope and a Nikon Equiphot-300 light microscope. Scanning-electron microscopy (SEM) and energy-dispersive x-ray (EDX) analysis were conducted using a Hitachi S-3000N SEM-EDX microscope.

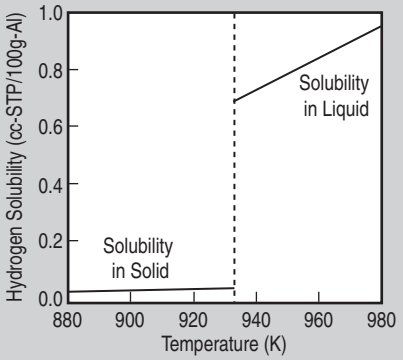

Figure 3. The variation in solubility of hydrogen with temperature in liquid and solid aluminum.[4]

Microporosity

As the name implies, microporosity (more often termed hydrogen-based porosity) relates to porosity that is relatively small in scale (<~300 μm in diameter). The mechanism of microporosity formation in aluminum alloy castings is complex, owing to its dependence on the interaction of a number of phenomena occurring during the manufacturing process including the pickup of hydrogen from the ambient air by liquid aluminum, the decrease in hydrogen solubility during solidification, behavior of oxide bifilms, volumetric shrinkage during solidification, and the development of the solidification structure.

Hydrogen pickup by liquid aluminum is a potential problem because the solubility of hydrogen is much greater in the liquid as compared to the solid. The variation in hydrogen solubility with temperature for aluminum[4] is shown in Figure 3. In the liquid phase, aluminum has a high affinity for oxygen and is able to crack (decompose) water vapor present in the ambient air according to the following reaction:

$$2Al_{(l)} + 3H_2O_{(g)} \Leftrightarrow Al_2O_{3(s)} + 6[H]_{Al} \quad (1)$$

The result is a gradual pickup of hydrogen with increased exposure to ambient air until the solubility limit is reached, ~0.69 cc H_2/100 g Al. In contrast, the solubility limit of solid aluminum is quite small, only ~0.036 cc H_2/100 g Al. As the liquid solidifies, any hydrogen within the solid in excess of the solubility limit is rejected into the liquid. If the concentration, or more specifically, the activity of hydrogen (measured in terms of partial pressure), exceeds the local pressure within the interdendritic liquid plus some amount associated with the nucleation event, then a hydrogen gas pore may form within the liquid. The result is a pore similar to the one shown in Figure 4.

The volume fraction (amount) and actual size of individual pores is not only influenced by the initial hydrogen content of the metal being cast, but also the local solidification conditions. The link between microporosity and solidification conditions stems from both the decrease in local pressure that occurs in the interdendritic liquid during the last stages of solidification and also the degree to which the solidified structure isolates pockets of liquid at high solid fractions.[5] The local pressure decrease develops because liquid is drawn into the mushy zone to compensate for the volumetric shrinkage associated with the liquid-to-solid transformation. Within the last regions to solidify (high solid fractions) this liquid must flow through material that is mostly solid and has a low permeability (high resistance to flow). Thus, the associated local pressure drop can be significant. Since the local pressure is now decreased, it is more probable that the hydrogen partial pressure will exceed the local pressure and consequently form porosity. Thus, conditions conducive to large interdendritic pressure drops, such as a long mushy zone and low thermal gradient within the wheel, can lead to an increase in the amount of microporosity formed.

Some of the most common quality issues associated with microporosity are cosmetic in nature as these defects form blemishes or irregularities on the painted surface of the wheel. Machined face wheels (i.e., those having a smooth machined surface as compared to an as-cast surface) are quite prone to this type of defect since the as-cast surface is removed during machining, exposing pores located just below the surface. Machined-face wheels typically also have high-luster paints, making surface irregularities more obvious to visual inspection.

Several examples of surface cosmetic defects are shown in Figure 5 for a machined wheel face finished with clear paint and for an as-cast wheel face finished with a silver/clear paint combination. Both macro-images (Figure 5a and 5c) of these defects and photomicrographs (Figure 5b and 5d) of the polished face surfaces showing the pore are presented.

In both of the examples shown, the surface cosmetic defects have microporosity associated with them. In the case of Figure 5b, the pore is seen to be intersecting the machined surface. Volatiles evolving from the paint coating can become trapped within this pore during the paint-bake cycle, leading to blistering on the painted surface. In the case of Figure 5d, the defect in the paint layer is right on top of the subsurface microporosity. Note the slight depression in the surface of the metal directly above the porosity. It is likely that at some location (below or above the plane examined) this cluster of microporosity intersected the surface and lead to the formation of a paint blister.

Figure 6 shows a series of hydrogen-based pores located in a wheel spoke just below the cast surface formed in a region with a 36 μm secondary dendrite arm spacing—corresponding to a cooling rate of approximately 1.5°C/s (the cooling rate during freezing has been estimated from the secondary dendrite arm spacing using an empirical formula for this alloy). The pores range in size from ~300 μm to ~450 μm. The three pores present are relatively spherical, as they all have a shape factor greater than 0.6 (shape factor of 1.0 is a sphere) and are all quite large. Although these pores are below the cast surface, there is a high probability that they would be exposed

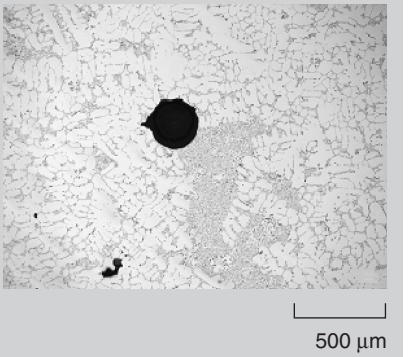

Figure 4. An example of hydrogen microporosity in LPDC A356 wheel.

during the surface-machining operation and could potentially result in cosmetic defects.

Microporosity can be particularly difficult to control in wheel-casting processes and often becomes problematic at certain times of the year. Industrial experience has shown that increased defects associated with microporosity in North American operations typically arise in June, July, August, and September. Figure 7 shows the annual variation of the partial pressure of water in the ambient air at a typical North American wheel casting facility (determined from knowledge of the ambient temperature and relative humidity). Clearly, the time frame of high microporosity coincides with the months of highest average partial pressure of water in the atmosphere and highest temperature. The combination of high temperature and relative humidity causes increased concentrations of hydrogen in the melt, leading to increased problems with microporosity.

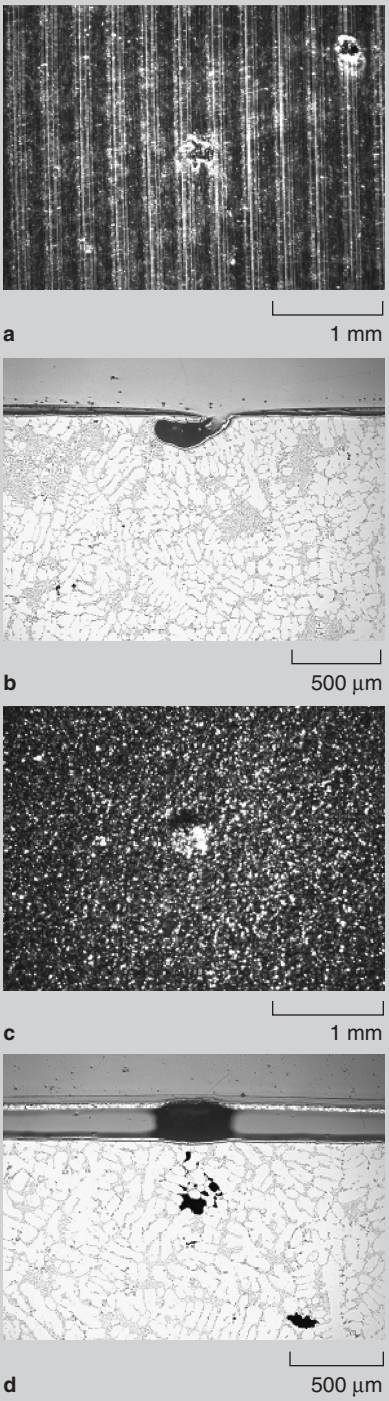

Figure 5. Macro-images of surface defects present on (a) machined and (c) as-cast surfaces of a wheel, and (b), (d) light microscope images showing the subsurface porosity and microstructure. The paint layer is shown in grey.

In addition to cosmetics, hydrogen-based porosity can affect the mechanical properties of a wheel—especially fatigue performance. Large pores can have a significant negative effect on fatigue life. Fatigue failure induced by porosity typically arises in sections of the wheel that see the largest in-service stresses, such as at the intersection of the spoke and hub. The size of pores necessary to affect fatigue performance depends on a combination of in-service and residual stresses present in the wheel (residual stresses develop in the wheel as a result of the quench step in the heat-treating operation). For example, a section within the wheel experiencing a high net tensile state of stress may be fatigue-life limited by relatively small pores, whereas a section experiencing only small net tensile stress would be fatigue-life limited by relatively large pores.

Figure 8 shows a series of larger hydrogen-based pores formed at the center of a spoke (far from the surface), in a region that has a secondary dendrite arm spacing of 62 μm, corresponding to a cooling rate of ~0.31°C/s. These pores range in size from 950 μm to 1,350 μm in the largest dimension. Note these are large pores and could be classified as either microporosity or macroporosity. However, these pores have not formed in clusters and possess a circular geometry, which would tend to suggest hydrogen-based porosity. These pores are sufficiently large that they could affect the fatigue performance of the wheel.

As shown in the series of defects presented in Figures 6 and 8, there is a clear trend of increasing pore size with increasing distance from the cast surface. Another feature worth noting is that the large pores within the center of the spoke are all associated with large pockets of eutectic liquid (the white structures in the photomicrographs are the primary aluminum structures that form first and the light grey structures are the Al-Si eutectic constituents that form during the last stage of solidification).

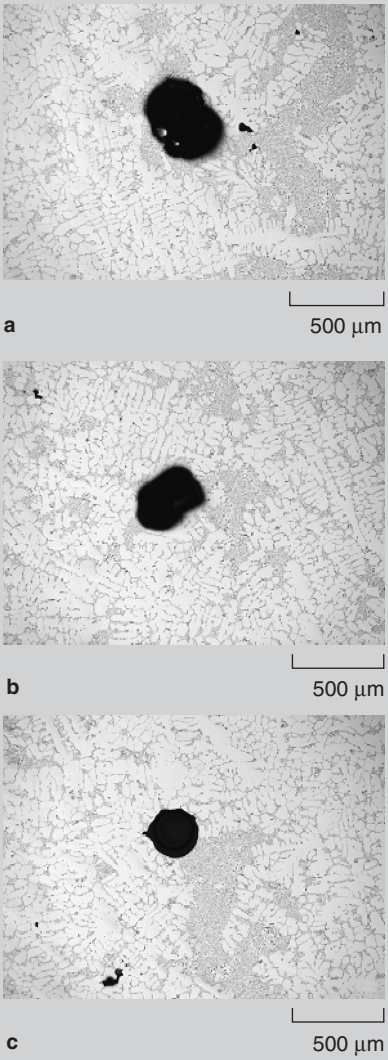

Figure 6. The hydrogen-based microporosity found in a spoke section and in proximity to the wheel-die interface. (a) ~460 μm diameter, (b) ~370 μm diameter, and (c) ~300 μm diameter.

Although considerable effort has been made to decrease and eliminate hydrogen-based micropores,[6–10] they remain the predominant defect in LPDC aluminum wheels. As the design envelope is

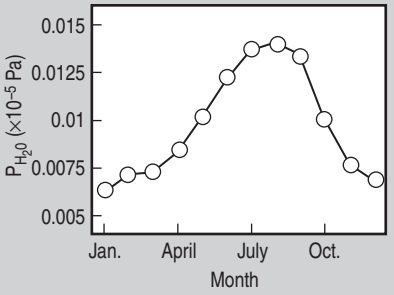

Figure 7. The annual variation in the ambient partial pressure of water at a typical North American wheel casting operation.

increased to further reduce weight and spoke area and increase wheel diameter, it is clear that control of microporosity formations and their effect on mechanical design must be better understood.

Over the past five decades, a significant amount of work has been carried out on the mechanisms of microporosity formation in aluminum alloy castings, principally through the development of mathematical models that simulate its formation.[11–24] Early models on predicting the local thermal environment during solidification (i.e., temperature gradient and freezing front velocity) yielded reasonable results on short freezing range alloys with low hydrogen content.[14,15] Most of the more recent numerical methods are well summarized in Lee's recent review.[16] The various approaches typically involve heat-transfer modeling coupled with hydrogen conservation equations, and expressions to predict the evolution in interdendritic pressure.[17–22] Recently, Rappaz and colleagues presented a "Mushy-Zone Refinement Method" to simulate Darcy flow and porosity formation.[23] Ohnaka and colleagues also presented a new method in which oxide entrapment during mold filling was simulated followed by the prediction of porosity formation during solidification by assuming that oxides entrapped inside the melt act as sites for pore nucleation.[24]

However, in practice, the ability to predict the size and location of dispersed microporosity is limited, particularly in complex industrial systems. For example, based on the images presented in Figures 6 and 8, it would appear that the formation of large pockets of eutectic has a significant role in determining the distribution and size of hydrogen-based porosity in addition to the local solidification conditions (temperature gradient and solidification velocity). Related studies have shown that large pockets of eutectic can affect the microstructure in a number of ways. First, these pockets can increase the porosity volume fraction and second, in non-grain-refined A356 castings, they can create an increase in the equivalent average pore diameter.[25] These pockets have been seen in strontium-modified A356 castings due to a decrease in eutectic nucleation frequency leading to eutectic clustering.[26] Although the link between increased porosity and strontium-based eutectic modification has been much reported,[25, 27–31] the exact mechanism and relationship is unclear. To date, no models incorporating the effect of eutectic cluster morphology on porosity have been published. The authors believe it will also be necessary to model the transport of hydrogen and interdendritic liquid to fully understand this aspect of pore formation.

Oxide Films

In the molten state, aluminum and its alloys oxidize immediately, forming a thin oxide film on the exposed surface of the metal. Excessive turbulence during mold filling can result in the entrainment of portions of this film within the cast metal and lead to the formation of a variety of defects.[6] For example, oxide films can act as stress concentrators and sites for fatigue crack initiation. In addition, it has been recognized that the crevasses formed by the folding of these films can act as nucleation sites for porosity and hot tearing.[6,32] Also, rim-leak defects are often associated with oxide films. It is likely that the entrainment of oxide films is related to flow characteristics, particularly the behavior of the liquid free surface, during die filling. Generally, these defects are small in size, indicating that there might be some small recirculation of the melt or localized surface turbulence when filling around obstructions within the dies. A simulation conducted on the filling sequence in LPDC aluminum wheels has shown evidence of some recirculation of molten metal in the hub face/sprue area and the hub/spoke area.[33] One possible counter measure would be to reduce the metal flow rate into the die, or alternately, to design the sprue/hub area so that turbulence is avoided. Another counter measure would be to leave the wheel in the die longer. Filtering and liquid metal quality within the holding furnace are also critical to avoid excessive oxide film entrainment.[34]

Figure 9 contains micrographs showing a cosmetic defect formed on the

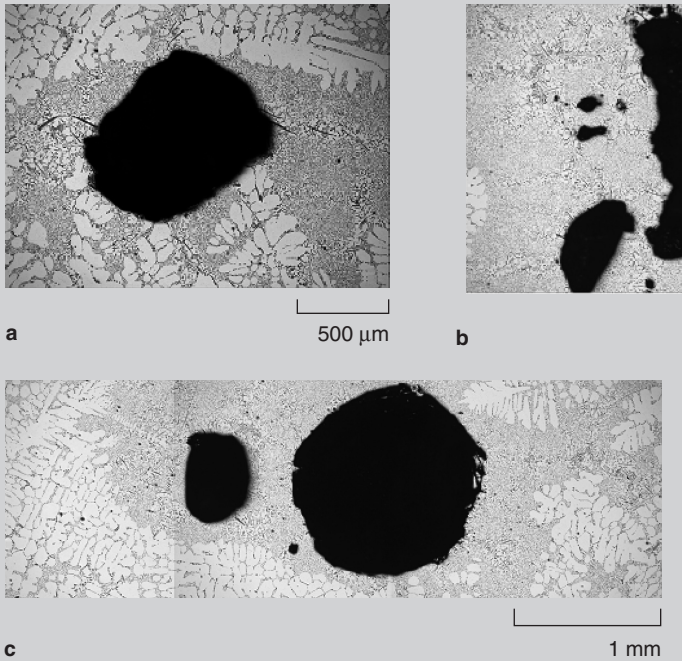

Figure 8. The hydrogen-based microporosity found in a spoke section and in proximity to center of the spoke. (a) ~996 μm diameter, (b) ~1,355 μm diameter, (c) ~1,260 μm diameter.

as-cast surface of a wheel in association with a trapped oxide film. As can be seen in Figure 9c, the oxide film has become delaminated at one end, leading to surface irregularities that can trap paint and cause the blister defect described previously (note the bubbles formed in the grey paint layer in association with the delaminated end of the entrapped oxide film). The mechanism by which the folded oxide film becomes delaminated is unclear, although it would appear that a layer of material was lifted up when the casting was ejected from the die. The oxide film is presumably weaker than the surrounding metal and hence it would fail when subjected to the tensile loading associated with wheel ejection.

Figure 10 shows a second example of an oxide-film-related cosmetic defect. As can be seen in the composite image, Figure 10c, the dent-like feature shown in Figure 10a is a gas pore in the paint layer that has intersected the surface of the paint. Figure 10c is a high-magnification micrograph of the cross section near the surface. This micrograph reveals a subsurface oxide film associated with this defect. Although, at this location, the oxide film does not appear to have fractured and pierced the surface (as in Figure 9c), it is possible that further grinding would reveal a region that had become separated and would be responsible for the pore in the paint.

Figure 11 shows an oxide film in relation to a rim leak defect. At the surface of the casting, the defect appears to be quite small and can only be detected visually with the aid of a die penetrant (Figure 11a). Figure 11b is an optical micrograph of the cross section of the rim, ~5 mm in thickness. In the image, the areas containing entrapped air and pores are white. As shown in Figure 11c, the entrapped air/pores are closely connected with an entrained and folded oxide film(s), running almost continuously through the cross section. The oxide film responsible for this defect likely formed elsewhere, such as in an area of turbulent flow in proximity to the sprue, or was entrained within the holding furnace and then became lodged within the rim.

Exogenous Inclusions

Exogenous inclusions are entrained particles not normally present in the alloy, arising from furnace linings, die components and coatings, and upstream processes. These particles include aluminum carbides (Al_4C_3), borides, and oxides. Depending on their location and size, and also on the wheel design, these inclusions can limit mechanical properties and fatigue performance as well as lead to cosmetic defects. Figure 12 shows an exogenous inclusion that resulted in a cosmetic defect on the surface of a machined face. As can be seen from the macro-image, Figure 12a, this defect appears to be very different than those previously examined. The light micrograph image, Figure 12b, confirms this to be an exogenous defect, which is surrounded partly by areas of oxide films and porosity.

As can be seen from the scanning-electron microscopy images, Figure 12c and d, the inclusion consists of at least three constituents: white particles, grey

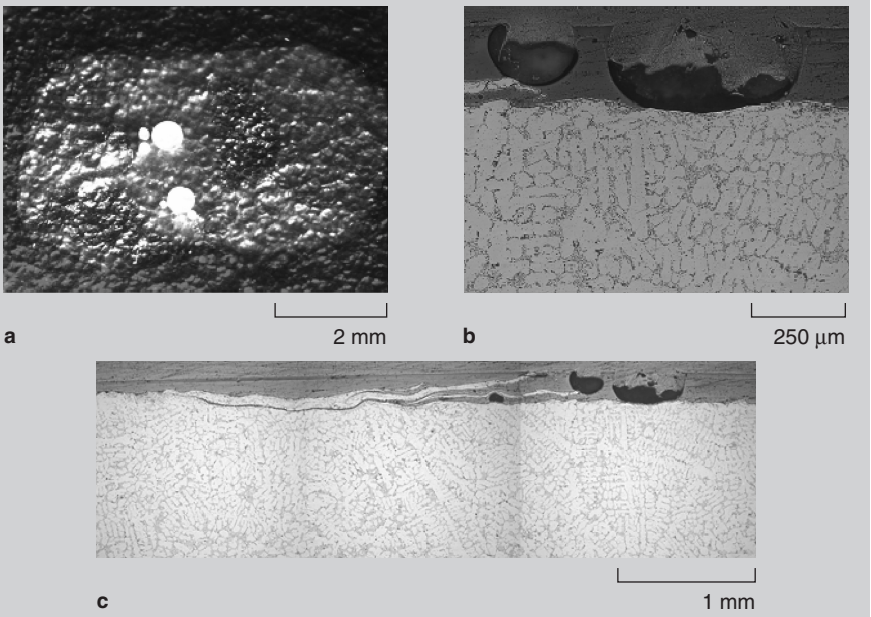

Figure 9. (a) A stereo-microscopic image of bright features and rough surface in association with folded oxide film; (b) composite light microscope image showing the oxide film layers; and (c) a high-magnification light microscope image of bubbles entrapped in the paint layer.

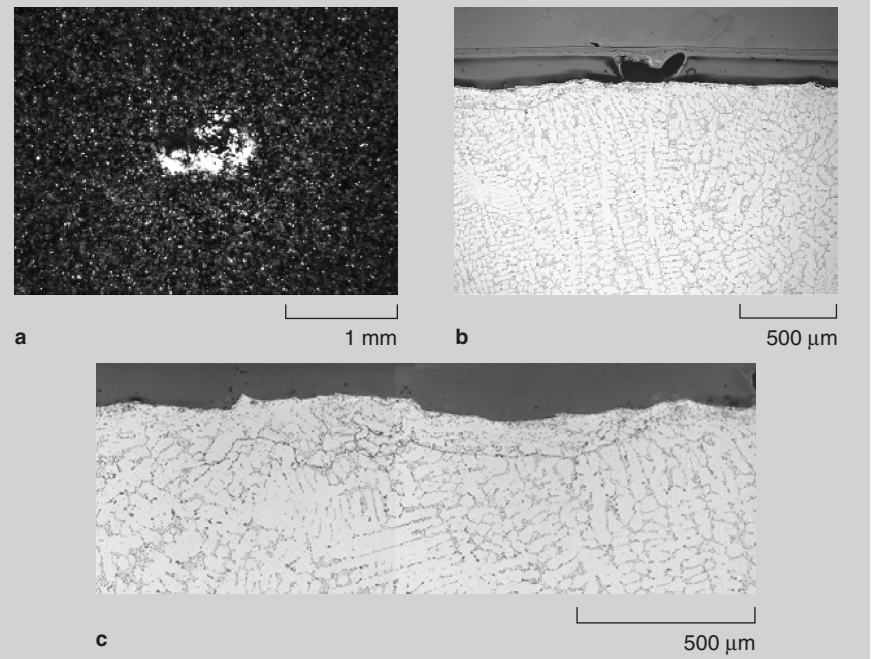

Figure 10. A stereo-microscope image of (a) defect area, (b) bubble in the paint layer associated with the underlying oxide film, and (c) subsurface oxide film associated with defect in the paint.

particles, and dark particles. An energy-dispersive x-ray (EDX) analysis of each of the particles revealed that the white particles are (all compositions in weight percent) $Al_xSi_yZr_zO_w$ (O-39.6Al-11.8Si-14.7Zr-32.3Mg-0.16Ca-0.72Ti-0.79); the grey particles are $Al_xSi_yO_z$ (O-46.8Al-50.2Si-1.84Mg-0.44Ca-037P-0.39); and the dark particles are $Al_xSi_yTi_z O_w$ (O-40.8Al-39.8Si-10.5Ti-5.4Mg-2.54Ca-1.04). It would appear that this is an exogenous inclusion (comprising at least some elements not present in the alloy) and thus could come from the die face coat or from the refractories present in the production system. Filters placed at the top of the sprue (entrance to the die cavity) have proven effective in removing these types of inclusions in previous studies.[34]

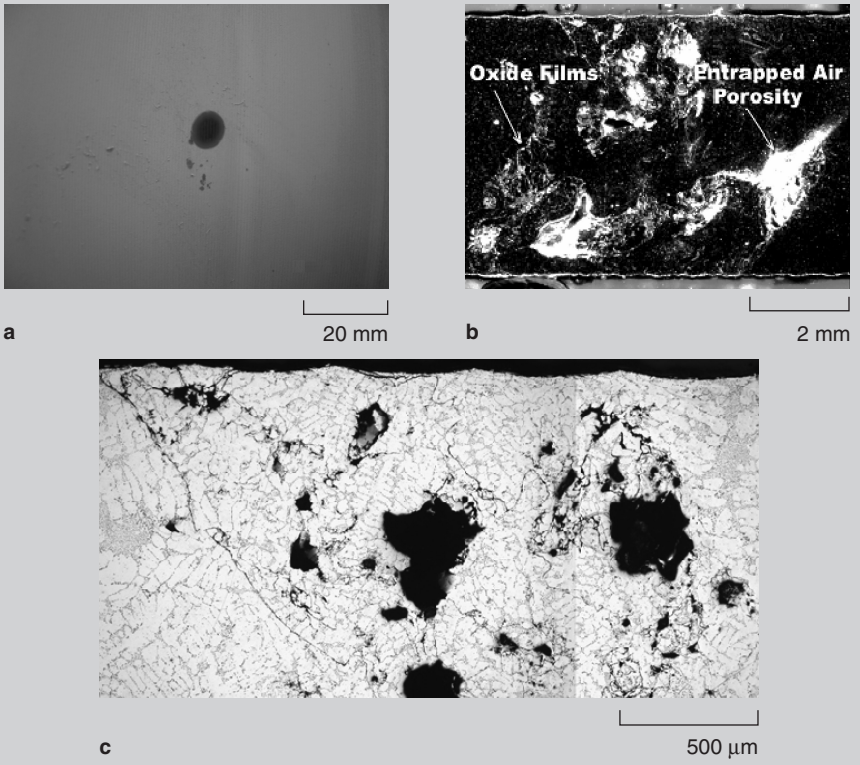

Figure 11. An image showing the rim leak defect area on the outside face of the wheel rim which has been delineated with (a) a die penetrant; (b) a stereo-microscope image of rim cross section at the leak defect; (c) a light microscopy image of the network of oxide films and pores in proximity to the outside face.

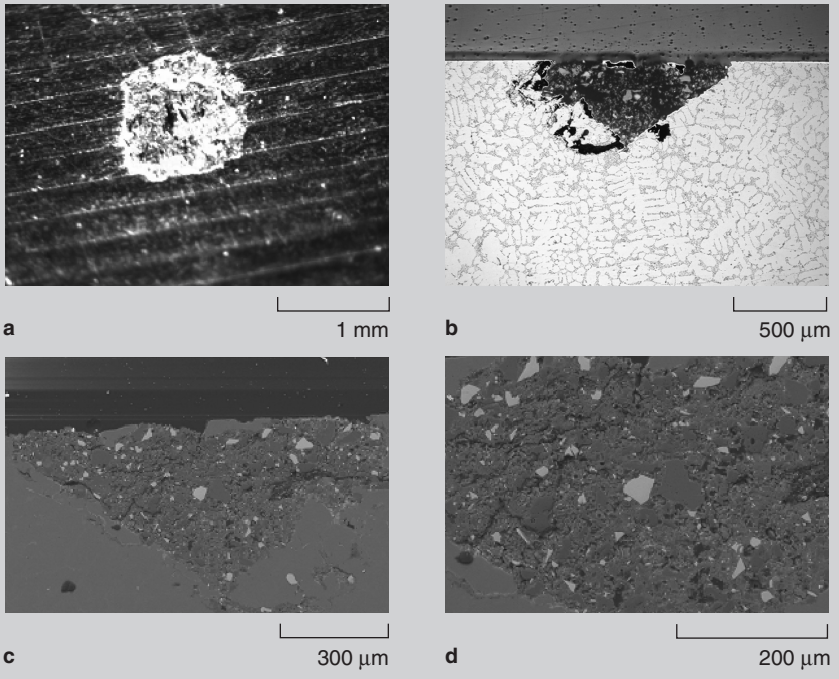

Figure 12. Stereo-microscope images of (a) a cosmetic defect on the machined surface; (b) a light microscope image of a sub-surface inclusion; (c) and (d) backscattered-electron and scanning-electron microscopy images of inclusion.

Influence of Casting Defects on Fatigue and Impact Performance

The poor fatigue performance of aluminum castings is the result of both a short fatigue crack initiation period and small crack propagation period which is exacerbated by the presence of pores, oxide inclusions, and oxide films.[35–45] Figure 13a and b shows fatigue crack initiation sites at a pore (Figure 13a) and at an oxide (Figure 13b).[39]

Numerous studies have investigated the impact of casting-related defects (porosity,[35–40] oxide films, and exogenous inclusions[37–40]) on the mechanical performance of cast alloys. Studies have also investigated the influence of microstructure (secondary dendrite arm spacing,[38,42] grain size,[43] silicon morphology,[41,42,44] and heat treatment[45]) on fatigue performance. A recent multi-scale computational model describing the fatigue behavior of cast aluminum alloys has greatly enhanced understanding of the relative contributions of porosity and microstructure on fatigue resistance.[46,47] In this study, the effect of pores was found to dominate over microstructure effects. Thus, in an industrial setting one might expect factors such as eutectic modification,[44] grain refining,[43] and heat treatment[45] to be overshadowed or dominated by casting-related defects in most instances.

In addition to fatigue testing, impact tests are also typically conducted during the preproduction stage to evaluate damage and eliminate the likelihood of failure and cracking under severe operating conditions. The impact performance is dependent not only on the section modulus and structural rigidity of the wheel, but also on the material properties such as elongation and impact strength. Thus, material microstructural and inhomogeneities such as defects (porosity/oxides) must be taken into account. There are limited reports on the effect of

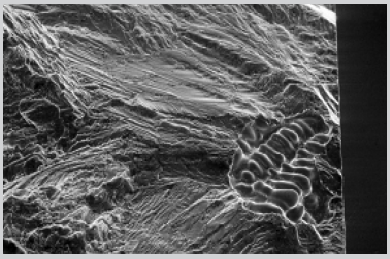

a 500 μm

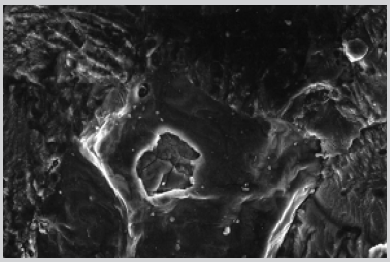

b 100 μm

Figure 13. SEM images showing the fatigue crack initiation at (a) a pore and (b) an oxide. All materials are strontium-modified A356-T6.[39]

defects on impact properties of wheels. One study on A356 shows that, although silicon morphology is the most influential factor on impact strength, porosity has some influence. At a hydrogen content of 0.2 cc/100 g, the impact strength of the strontium-modified alloy was reduced by 20% because of the porosity.[48]

CONCLUSIONS

Casting-related defects in LPDC aluminum wheels, including macroporosity and microporosity, oxide films, and exogenous inclusions, continue to challenge production engineers and metallurgists, particularly within an environment where the demands on performance continue to increase. From a production point of view, cosmetic defects relating to hydrogen-based porosity and oxide films are the most critical. However, the greater challenge lies in developing an integrated approach to wheel structural performance (both fatigue and impact) that includes consideration of casting-related defects. The cost of redesigning a wheel and the associated die tooling when a significant portion of the manufactured wheels fail to meet mechanical performance criteria following preproduction trials is prohibitively expensive.

To meet this challenge, additional work of a more fundamental nature is required. This includes investigating the effect of alloy modification and interdendritic fluid flow on eutectic cluster size, eutectic cluster distribution, porosity nucleation, and porosity growth. In addition, work of a more applied nature is required in which the emphasis is placed on integration of current scientific knowledge into mathematical process models that will be of practical use to production engineers. This model is at a stage of sophistication where a more holistic approach to product design can begin, whereby not only are the casting process and the associated defects modeled, but their downstream impact on product performance is also included.

ACKNOWLEDGEMENTS

The authors would like to acknowledge financial support from the Natural Sciences and Engineering Research Council of Canada. The authors thank Jacobsen Real-Time X-ray Machinery for the radiography on the wheels. One of the authors (B.Z.) is very grateful to Dr. J.T. Berry of Mississippi State University for his valuable comments.

References

1. F. Chiesa, *AFS Trans.*, 103 (1995), pp. 547–554.
2. J. Nath, *SAE Technical Paper Series 950723* (SP-1097) (Warrendale, PA: SAE International, 1995), pp. 75–90.
3. D. Argo and J.E. Gruzleski, *AFS Trans.*, 96 (1988), pp. 65–74.
4. M.C. Fleming, *Solidification Processing* (New York: McGraw-Hill Inc., 1974), p. 204.
5. J.D. Zhu et al., *Int. J. Cast Metal Res.*, 18 (2005), pp. 229–235.
6. J. Campbell, *Castings* (Oxford, U.K.: Butterworth-Heinemann, 1991), pp. 1–26, 261–263.
7. J.T. Berry and R. Taylor, *AFS Trans.*, 107 (1999), pp. 203–206.
8. A. Dahle, L. Arnberg, and D. Apelian, *AFS Trans.*, 105 (1997), pp. 963–970.
9. C. Frueh et al., *Proceedings from the 2nd International Aluminum Casting Technology Symposium* (Materials Park, OH: ASM International, 2002), pp. 99–105.
10. B. Zhang, R. Luck, and J.T. Berry, *AFS Trans.*, 112 (2004), pp. 237–250.
11. T.S. Piwonka and M.C. Flemings, *AIME Met. Soc. Trans.*, 236 (1966), pp. 1157–1165.
12. J. Campbell, *Trans. of the Metall. Soc. of AIME*, 245 (1969), pp. 2325–2334.
13. D.R. Poirier, K. Yeum, and A.L. Maples, *Metall. Trans. A*, 8A (1987), pp. 1979–1987.
14. E. Niyama et al., *AFS Int. Cast Metals J.*, 6 (1981), pp. 16–22.
15. V.K. Suri et al., *AFS Trans.*, 100 (1992), pp. 399–408.
16. P.D. Lee, A. Chirazi, and D. See, *J. of Light Metals*, 1 (2001), pp. 15–30.
17. K. Kubo and R.D. Pehlke, *Met. Trans. B*, 16B (1985), pp. 359–366.
18. J.D. Zhu and I. Ohnaka, *Modelling of Casting, Welding and Advanced Solidification Processes V,* ed. M. Rappaz, M.R. Ozgu, and K.W. Mahin (Warrendale, PA: TMS, 1991), pp. 435–441.
19. G.K. Sigworth and C. Wang, *Metal Trans. B*, 24B (1993), pp. 349–364.
20. J. Huang, J.G. Conley, and T. Mori, *Metal. Trans. B,* 29 (1998), pp. 1249–1260.
21. S.D. Felicelli, D.R. Poirier, and P.K. Sung, *Metall. & Mater. Trans. B*, 31B (2000), pp. 1283–1292.
22. P. Vo et al., *Light Metals 2001*, ed. J.L. Anjier (Warrendale, PA: TMS, 2001), pp. 1115–1121.
23. Ch. Pequet, M. Gremaud, and M. Rappaz, *Metall. & Mater. Trans A.,* 33A (2002), pp. 2095–2106.
24. Y. Sako et al., *Proc. of the 7th Asian Foundry Congress*, ed. Y.N. Pan (Kaohsiung, Taiwan: Chinese Foundreymen's Assn., 2001), pp. 363–369.
25. Q.T. Fang and D.A. Granger, *Light Metals 1989*, ed. P.G. Campbell (Warrendale, PA: TMS, 1989), pp. 927–935.
26. L. Lu et al., *JOM*, 56 (11) (2004), pp. 52–58.
27. B. Closset and J.E. Gruzleski, *Metall. Trans. A*, 13A (1982), pp. 945–951.
28. Q.T. Fang and D.A. Granger, *AFS Trans.*, 97 (1989), pp. 989–1000.
29. K. Tynelius, J.F. Major, and D. Apelian, *AFS Trans.*, 101 (1993), pp. 401–413.
30. J.P. Anson, M. Stucky, and J.E. Gruzleski, *AFS Trans.*, 108 (2000), paper 00-70.
31. S.D. McDonald et al., *AFS Trans.*, 108 (2000), paper 00-115.
32. S. Fox and J. Campbell, *Int. J. Cast Metals Res.*, 14 (6) (2000), pp. 335–340.
33. D.P.K. Singh et al., *AFS Trans.*, 107 (1999), pp. 127–133.
34. T.K. Loughnane, D.P.K. Singh, and D.L. Zhang, *AFS Trans.,* 111 (2003), paper 03-118.
35. M.J. Couper, A.E. Neeson, and J.R Griffiths, *Fatigue Fract. Engng. Mater. Struct.*, 13 (1990), pp. 213–227.
36. J.M. Boileau, J.W. Zindel, and J.E. Allison, *SAE Paper 970019* (Warrendale, PA: SAE International, 1997).
37. C. Nyahumwa, N.R. Green, and J. Campbell, *Advances in Aluminum Casting Technology*, ed. M. Tiryakioglu and J. Campbell (Materials Park, OH: ASM International, 1998), pp. 225–234.
38. J.F. Major, *AFS Trans.*, 106 (1998), pp. 901–906.
39. B. Zhang, D.R. Poirier, and W. Chen, *Metall. Mater. Trans. A*, 30A (1999), pp. 2659–2666.
40. Q.G. Wang, D. Apelian, and D.A. Lados, *J. of Light Metals*, 1 (2001), pp. 73–84.
41. B. Zhang et al., *AFS Trans.*, 108 (2000), pp. 383–389.
42. Q.G. Wang, D. Apelian, and D.A. Lados, *J. of Light Metals*, 1 (2001), pp. 85–97.
43. G.E. Byczynncki and D.A. Cusinato, *Int. J. of Cast Metals Res.*, 14 (2002), pp. 315–324.
44. B. Zhang, D.R. Poirier, and W. Chen, *AFS Trans.*, 110 (2002), pp. 393–405.
45. C.J. Davidson, J.R. Griffith, and A.S. Machin, *Fatigue Fract. Engng. Mater Struct*, 25 (2002), pp. 223–230.
46. J.H. Fan et al., *Engng. Fract. Mech.*, 68 (2001), pp. 1687–1706.
47. D.L. McDowell et al., *Engng. Fract. Mech.,* 70 (2003), pp. 49–80.
48. W. LaOchan and J.E. Gruzleski, *AFS Trans.*, 100 (1992), pp. 415–424.

B. Zhang, S.L. Cockcroft, D.M. Maijer, J.D. Zhu, and A.B. Phillion are with the Department of Materials Engineering at the University of British Columbia in Vancouver, Canada.

For more information, contact B. Zhang, the University of British Columbia, Department of Materials Engineering, #401B, 6350 Stores Road, Vancouver, BC, Canada V6T 1Z4; (604) 827-5345; fax (604) 822-3619; e-mail bzhang@cmpe.ubc.ca.